Hollow Polyhedral Structures in Small Gold−Sulfide Clusters

Yong Pei,[†,‡,*] Nan Shao,[§] Hui Li,[†] De-en Jiang,[§,*] and Xiao Cheng Zeng[†,*]

[†]Department of Chemistry and Nebraska Center for Materials and Nanoscience, University of Nebraska-Lincoln, Lincoln, Nebraska 68588, [‡]Department of Chemistry, Key Laboratory of Environmentally Friendly Chemistry and Applications of Ministry of Education, Xiangtan University, Hunan Province, P. R. China, 411105, and [§]Chemical Sciences Division, Oak Ridge National Laboratory, Oak Ridge, Tennessee 37831

ABSTRACT Using *ab initio* methods, we investigate the structural evolution of a family of gold−sulfide cluster anions ($Au_mS_n^-$). We show that this family of clusters exhibits simple size-evolution rules and novel hollow polyhedron structures. The highly stable $Au_mS_n^-$ species such as $Au_6S_4^-$, $Au_9S_5^-$, $Au_9S_6^-$, $Au_{10}S_6^-$, $Au_{11}S_6^-$, $Au_{12}S_8^-$, and $Au_{13}S_8^-$ detected in the recent ion mobility mass spectrometry experiment of $Au_{25}(SCH_2CH_2Ph)_{18}$ (Angel *et al*. *ACS Nano* 2010, *4*, 4691) are found to possess either quasi-tetrahedron, pyramidal, quasi-triangular prism, or quasi-cuboctahedron structures. The formation of these polyhedron structures are attributed to the high stability of the S−Au−S structural unit. A unique "edge-to-face" growth mechanism is proposed to understand the structural evolution of the small $Au_mS_n^-$ cluster. A 3:2 ratio rule of Au/S is suggested for the formation of a hollow polyhedron structure among small-sized Au_mS_n clusters.

KEYWORDS: gold−sulfide cluster anions ($Au_mS_n^-$) · hollow polyhedron structures · *ab initio* methods · basin-hopping · global minima · edge-to-face evolution mechanism

Platonic polyhedra such as tetrahedron, cube, octahedron, dodecahedron, and icosahedron are highly symmetric structural motifs that can appear not only in transition-metal coordination compounds[1] but also in atomic and molecular clusters in the form of *hollow* polyhedral moieties. Understanding the physical and chemical properties of the polyhedron-motif based atomic and molecular clusters is one of central tasks in cluster science.[2] The Wade's $2(n+1)$ electron rule has been used to predict the polyhedral structure of nonmetal clusters, particularly, electron deficient clusters such as *closo* boranes and carbranes.[3] More general rules (such as $4n$, $5n$, $6n$, and $8n$ electrons rules) have been developed by Mingos *et al*. to understand and to predict structures of various main-group atomic clusters and transition-metal clusters. These rules are considered as the polyhedral skeleton electron pair approach.[4] The Wade's rules have also been used to guide experimental synthesis of endohedral or hollow Zintl ions.[5−7] One example of the Zintl ions is the Pb_{10}^{2-} dianion which features a capped square antiprismatic structure with 22 bonding skeletal electrons.[8] Moreover, the gas-phase icosahedral tin and lead Zintl ions Sn_{12}^{2-} (stannaspherene)[9] and Pb_{12}^{2-} (plumbaspherene)[10] have been detected in the photoelectron spectroscopy measurements. A number of endohedral Zintl-ion containing structures have also been synthesized in the solution and solid phase.[11]

Contrary to the main-group element clusters, the ligand-free noble metal clusters rarely exhibit hollow polyhedral structures. One exception is the gold cluster anions in the size range of 16−18,[12] which have been detected experimentally to exhibit hollow polyhedral structures due in part to the strong relativistic effect of Au.[13−15] Other stable or metastable hollow-cage structures in the size range of Au_{32}−Au_{72} have been predicted theoretically.[16−20] Moreover, the formation of hollow cages supported on the MgO has been investigated using *ab initio* calculations.[21] Can ligated noble-metal clusters exhibit hollow polyhedral structures? To our knowledge, few studies on this topic have been reported in the literature. We note however that thiolate (-SR)-stabilized gold clusters have been extensively studied both experimentally and theoretically.[22−36] A recent XRD study of the single crystal of thiolated gold clusters reveals that many of these clusters have an Au-core protected by the "staple" motifs (*e.g.*, −SR−Au−SR− and −SR−Au−SR−Au−SR−, *etc.*) The high stability of chainlike −SR−Au−SR− and −SR−Au−SR−Au−SR− "staple" motifs suggests that they can be building units for aggregates and even afford special polyhedral structures. Indeed, the −[SR−Au]− polymers have been reported.[37,38] In addition, many small thiolate-gold molecules $(Au-SR)_N$ exhibit catenane, helix, and puckered ring structures.[39,40]

*Address correspondence to ypnku78@gmail.com, jiangd@ornl.gov, xczeng@phase2.unl.edu.

Received for review November 25, 2010 and accepted January 12, 2011.

Published online January 27, 2011
10.1021/nn103217z

Recent progress in synthesizing monodisperse thiolated gold clusters also allows access of a wide size range of Au_mS_n clusters. For example, during ionization of $Au_{25}(SR)_{18}$ in matrix−assisted laser desorption/ionization (MALDI) mass spectrometry (MS), a series of $Au_mS_n^-$ clusters were produced in the gas phase from the fragmentation of $Au_{25}(SR)_{18}$.[41] Among them, the monoanionic clusters $Au_{25}S_{12}^-$, $Au_{23}S_{11}^-$, and $Au_{27}S_{13}^-$ exhibit high stability. Fast-atom-bombardment MS of $Au_{25}(SR)_{18}$ in both positive and negative modes revealed complex patterns of fragmentation, including formation of many $Au_mS_n^+$ and $Au_mS_n^-$ clusters.[42] More recently, ion-mobility MS of $Au_{25}(SR)_{18}$ showed high abundance (magic number) of smaller $Au_mS_n^-$ clusters such as $Au_{13}S_8^-$, $Au_{12}S_8^-$, and down to $Au_6S_4^-$.[43] Coincidentally, the laser desorption mass spectrum of subnanometer gold clusters made from meso-2,3-dimercaptosuccinic acid also showed high abundances of $Au_mS_n^-$ clusters around $Au_{13}S_8^-$ and down to $Au_7S_5^-$, together with some abundances around $Au_{25}S_{12}^-$.[44] More interestingly, negative-mode MALDI MS of $Au_4L_3^-$ and $Au_4L_4^-$ (L = 2, 3-dimercaptopropanesulfonate) clusters showed continuous growth of $Au_mS_n^-$ clusters from $Au_6S_4^-$ to $Au_{25}S_{12}^-$ with decreasing abundance.[45] Although structures of $Au_{25}S_{12}^-$, $Au_{23}S_{11}^-$, and $Au_{27}S_{13}^-$ were predicted to be core-in-cage like where the Au core is encapsulated in a series of Au_mS_n cages composed of S−Au−S edges,[46] how the small-sized $Au_mS_n^-$ clusters evolve their structures and what role the S−Au−S unit plays there are still open questions. Motivated by these previous studies as well as by gas-phase experimental and *ab initio* calculation studies of high stability of the chain-like S−Au−S specie,[47−50] we have explored the most stable structures of small-sized $Au_mS_n^-$ clusters (m from 1 and up to 15) and determined their size-evolution patterns based on these highly stable structures. Remarkably, a number of hollow polyhedral structures among small-sized $Au_mS_n^-$ are revealed, for the first time, based on the global minimum search. These hollow polyhedral structures are composed of simple S−Au−S edges and show simple size-evolution rules. The magic-number clusters such as $Au_6S_4^-$, $Au_9S_5^-$, $Au_9S_6^-$, $Au_{10}S_6^-$, $Au_{11}S_6^-$, $Au_{12}S_8^-$, and $Au_{13}S_8^-$, found in MS of several different thiolated gold nanoclusters,[41−45] are predicted to have polyhedron structures such as quasi-tetrahedron, pyramidal, quasi-triangular prism, or quasi-cuboctahedron with or without an encapsulated Au atom.

RESULTS AND DISCUSSION

To investigate structural evolution of gold-sulfide monoanionic clusters ($Au_mS_n^-$), a large population of low-energy isomers for each size are generated and optimized using a combined density functional theory (DFT)[51,52] and the basin-hopping global optimization method.[53] The details are given in the Computational Methods section.[54−62] Notably, several hollow polyhedral structures that are built upon the S−Au−S edges, including the tetrahedron, triangular prism, pentagonal prism, and capped pyramid, are found to be energetically low-lying isomers. In Figure 1a, we show the smallest cluster AuS_2^- has a linear geometry with Au locating in the middle. This linear cluster possesses a triplet spin ground state. With adding more Au and S atoms, the $Au_mS_n^-$ clusters turn into near-triangular and near-square structures at the size of $Au_3S_3^-$ and $Au_4S_4^-$ (*cf.* Figure 1a), respectively. Note that the triangle or square is a basic face of polyhedrons. With more and more Au and S atoms, several hollow polyhedral structures of $Au_mS_n^-$ clusters are found. We classify these hollow polyhedral structures in three groups.

Polyhedral Structures with Shared 3-Coordinated S Vertexes. As shown in Figure 1b, clusters $Au_6S_4^-$, $Au_7S_5^-$, $Au_9S_6^-$, $Au_{10}S_6^-$, $Au_{11}S_6^-$, $Au_{12}S_7^-$, $Au_{12}S_8^-$, and $Au_{13}S_8^-$ exhibit polyhedral structures with shared 3-coordinated S atom. Among them, one may find the $Au_6S_4^-$ (C_{2v}), $Au_9S_6^-$ (C_{2v}) and $Au_{12}S_8^-$ (D_{4h}) exhibit *hollow* quasi-tetrahedron, quasi-triangular prism, and quasi-cuboctahedron structures (highlighted by the green background), respectively. Both density-functional theory (DFT) and MP2 calculations indicate that the quasi-tetrahedron and quasi-triangular prism structures of $Au_6S_4^-$ and $Au_9S_6^-$ are more stable than the second lowest-lying isomers by 1.28 and 0.43 eV at the TPSS//cc-pVTZ level, and 1.73 and 0.84 eV at the MP2//cc-pVTZ level, respectively. We note that $Ag_6S_4^-$ was also predicted to have a similar quasi-tetrahedron structure.[63] For the quasi-cuboctahedron $Au_{12}S_8^-$, the energy difference between the hollow and core-stacked isomers is 0.50 eV (at MP2//cc-pVTZ level). The $Au_{10}S_6^-$, $Au_{11}S_6^-$, and $Au_{13}S_8^-$ have one Au atom encapsulated in the hollow space of the polyhedron structures. Especially, the $Au_{13}S_8^-$ has the Au-doped cuboctahedron structure which is more stable than the face-capped isomer by 1.26 eV (*cf.* Supporting Information), suggesting higher stability of the core-doped polyhedron structure.

Polyhedron Structures with Mixed Au and S Vertexes. An Au atom may replace a vertex S atom to form polyhedral structures when the number ratio of Au/S is greater than 3:2, for example, $Au_7S_3^-$, $Au_9S_4^-$, $Au_{10}S_4^-$, $Au_{10}S_5^-$, and $Au_{11}S_5^-$ shown in Figure 1b. Among them, the $Au_7S_3^-$ and $Au_{10}S_5^-$ exhibit hollow quasi-tetrahedral and triangular prism-like structures (highlighted by the aqua background), similar to those of iso-atomic-number clusters $Au_6S_4^-$ and $Au_9S_6^-$. However, one vertex S atom is replaced by an Au atom in these structures, which results in two types of polyhedron edge, that is, S−Au−S and Au−Au−S. The $Au_{11}S_5^-$ has the same polyhedron framework as $Au_{10}S_5^-$. An extra Au atom is filled into the hollow space of $Au_{11}S_5^-$. We find the core-doped structure of $Au_{11}S_5^-$ is much more stable

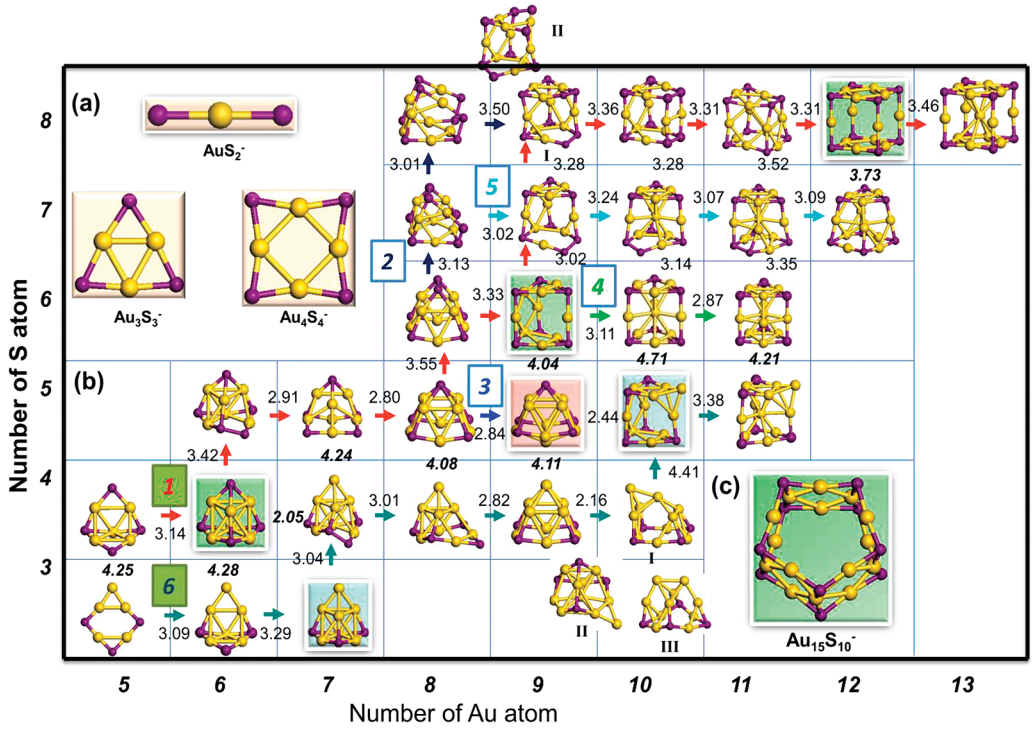

Figure 1. A chart to illustrate structural evolution of small $Au_mS_n^-$ cluster anions. Arrows with different colors indicate different size-evolution routes: (red arrow) route 1, (black arrow) route 2, (blue arrow) route 3, (light green arrow) route 4, (blue arrow) route 5, and (dark green arrow) route 6. The value associated with each arrow is the formation energy (eV), which is defined by $E_{form} = E(Au_mS_n^-) - E(Au_mS_{n-1}^-) - E$(S atom) or $E_{form} = E(Au_mS_n^-) - E(Au_{m-1}S_n) - E$(Au atom). Purple spheres represent S atoms, and yellow spheres refer to Au. Green and blue background colors are to highlight the hollow polyhedral structures. The clusters highlighted by light-green or blue background are iso-atomic clusters with the same structural feature.

than the face-capped isomer structure by 0.81 eV (*cf.* Supporting Information), suggesting again the preference of the formation of doped polyhedron structures with excess Au atoms.

Pyramid Structure with 4-Coordinated S Atom Vertex. A unique pyramidal structure is found for $Au_9S_5^-$ and $Au_8S_5^-$, respectively, with or without being bottom-capped by a Au atom (*cf.* Figure 1b), where the top-vertex S atom is tetra-coordinated. These pyramidal structures exhibit the C_{4v} symmetry with four identical triangular Au_3S_3 faces and a square Au_4S_4 face at the bottom. In the $Au_9S_5^-$ (highlighted by pink background), the bottom Au_4S_4 face is capped by an Au-atom and the whole cluster is viewed as a hollow pyramidal cage. Note that the $Au_9S_5^-$ can also form the triangular bipyramidal (deltahedron) structure, which is less stable than the bottom-capped pyramidal structure by 0.64 eV at the MP2//cc-pVTZ level (*cf.* Supporting Information).

To understand the size-evolution of these polyhedral structures, we systematically study a number of low-lying structures of $Au_mS_n^-$ with various Au and S ratios. Figure 1b lists the lowest-energy structures confirmed at both TPSS//cc-pVTZ and MP2//cc-pVTZ levels of theory (*cf.* minima list in Supporting Information). On the basis of the obtained structures, six size-evolution routes (**1**−**6**) are identified and illustrated by colored arrows in Figure 1b, which start from either $Au_5S_3^-$ or $Au_5S_4^-$ and end at $Au_9S_5^-$, $Au_{11}S_5^-$, $Au_{11}S_6^-$, $Au_{12}S_7^-$, or $Au_{13}S_8^-$. The structural evolution of $Au_mS_n^-$ clusters from the simple S−Au−S unit to various hollow polyhedral cages, and then to the core-stacked structures, can be clearly recognized.

Starting from $Au_5S_4^-$, the addition of an Au atom will connect two separated S atoms, result in an S−Au−S edge ($Au_5S_4^- \rightarrow Au_6S_4^-$), and form the *quasi*-tetrahedron $Au_6S_4^-$. The *quasi*-tetrahedron $Au_6S_4^-$ is composed of four Au_3S_3 triangular faces, which can evolve into *quasi*-cuboctahedron $Au_{12}S_8^-$ (composed of six square Au_4S_4 faces) through a *quasi*-triangular prism intermediate $Au_9S_6^-$ (composed of mixture of triangle and square faces) along route **1**. Route **2** branches from route **1** at $Au_8S_6^-$ and then merges into route **1** at $Au_9S_8^-$. Note that for the $Au_9S_8^-$, two isoenergetic structures $Au_9S_8^-$ (**I**) and $Au_9S_8^-$ (**II**) are found, which has the energy difference of 0.02 eV at MP2//cc-pVTZ level. The two isomers are different in the orientation of two disulfide bonds. The $Au_9S_8^-$ (**I**) can be built from either $Au_8S_8^-$ or $Au_9S_7^-$ through the insertion of an Au atom or formation a new disulfide bond. Moreover, starting form $Au_9S_8^-$ (**I**), the addition of an Au atom may connect two separated S atom to reach the structure of $Au_{10}S_8^-$ (cf. Figure 1b). However, due to the different orientation of two disulfide bonds,

the structure of $Au_9S_8^-$ (**II**) cannot directly evolve into the structure of $Au_{10}S_8^-$ by addition of an Au atom.

In route **1**, the intermediate cluster $Au_8S_5^-$ is composed of four triangular Au_3S_3 faces and one square Au_4S_4 face, which exhibits a pyramid like structure. From $Au_8S_5^-$, the addition of an Au atom leads to a branch route, denoted as route **3**. An Au atom is attached to the center of square Au_4S_4 face in $Au_8S_5^-$, which results in a unique bottom-capped pyramid-like structure ($Au_9S_5^-$). Route **3** is ended at $Au_9S_5^-$.

Route **4** branches from route **1** at $Au_9S_6^-$. Here, an extra Au atom will fill the inner hollow space of $Au_9S_6^-$ ($Au_9S_6^- \rightarrow Au_{10}S_6^-$), and then an additional Au atom will attach to one of square Au_4S_4 face on the *quasi*-triangular prism unit ($Au_{10}S_6^- \rightarrow Au_{11}S_6^-$).

Route **5** branches from route **2** at $Au_8S_7^-$. Here, the continuous addition of Au atoms will eventually lead to a core-stacked structure of $Au_{12}S_7^-$. It is worth noting that from $Au_9S_7^- \rightarrow Au_{10}S_7^-$ in route **5**, the added Au atom prefers to fill the hollow space of the cage rather than inserting a disulfide bond. However, the disulfide bond insertion mechanism is still very competitive compared to the cage fill process, as the cage-like isomer is close in energy to the core-stacked isomer for $Au_{10}S_7^-$ (*cf.* Supporting Information).

Route **6** depicted in Figure 1b starts from $Au_5S_3^-$, which is independent of the other five routes as it has no cross with routes **1**−**5**. An extra Au atom added to $Au_5S_3^-$ ($Au_5S_3^- \rightarrow Au_6S_3^-$) will connect two separated S atoms in $Au_5S_3^-$ and lead to the formation of a new kind of Au_4S_2 triangular face. Following route **6**, a tetrahedron- like structure is formed upon the increase of Au atom ($Au_6S_3^- \rightarrow Au_7S_3^-$). The structural evolution from $Au_7S_3^-$ to $Au_8S_4^-$ involves the formation of a disulfide bond and consequent insertion of an Au atom. A square Au_4S_4 face is formed in $Au_8S_4^-$. From $Au_8S_4^-$ to $Au_9S_4^-$, the added Au atom will connect the separated Au and S atoms to form a new Au−Au−S edge. The $Au_9S_4^-$ thus has four Au_4S_2 triangular faces and one square Au_4S_4 face, which exhibits pyramid-like structure. However, unlike the step $Au_8S_5^- \rightarrow Au_9S_5^-$ in route **3**, the addition of an Au atom to $Au_9S_4^-$ ($Au_9S_4^- \rightarrow Au_{10}S_4^-$) will not lead to the formation of a bottom-capped pyramid cage structure. For the $Au_{10}S_4^-$, the TPSS//cc-pVTZ and MP2//cc-pVTZ calculations yield different relative stabilities among local-minimum structures. As seen from the Supporting Information, the TPSS//cc-pVTZ calculation suggests that hollow structure **I** is slightly more stable than the core-stacked isomer **II** or the hollow structure **III**. However, the core-stacked isomer $Au_{10}S_4^-$(**II**) is more stable than $Au_{10}S_4^-$(**I**) or $Au_{10}S_4^-$(**III**) by 0.75 and 0.16 eV, respectively, according to the MP2//cc-pVTZ calculation. From Figure 1b, both $Au_{10}S_4^-$ (**I**) and (**III**) may be viewed as the attachment of an added Au atom to a triangular Au_3 unit on the top of $Au_9S_4^-$. And the transition of $Au_{10}S_4^-$(**I**) or $Au_{10}S_4^-$(**III**) $\rightarrow Au_{10}S_5^-$ can be viewed as the attachment of an S atom to a triangular Au_3 unit in $Au_{10}S_4^-$(**I**) or $Au_{10}S_4^-$(**III**) (forming a new Au−Au−S edge and two S−Au−S edges). However, the core-stacked isomer $Au_{10}S_4^-$(**II**) may not act as a linker between structures of $Au_9S_4^-$ and $Au_{10}S_5^-$ in route **6**. Finally, the addition of an Au atom to $Au_{10}S_5^-$ results in a core-stacked structure $Au_{11}S_5^-$ ($Au_{10}S_5^- \rightarrow Au_{11}S_5^-$). The vertical detachment energy (VDE) of electron for all anionic clusters shown in Figure 1b and the photoelectron spectrum for some near iso-energetic isomers such as $Au_9S_8^-$ (**I**−**II**) and $Au_{10}S_4^-$ (**I**−**III**) are calculated at the TPSS//cc-pVTZ level (see Supporting Information,Table S1 and Figure S1). As seen in Table S1, the $Au_mS_n^-$ cluster anions possess quite large VDE values (>3.78 eV). Moreover, the difference in the photoelectron spectrum calculated for isomers of $Au_9S_8^-$ (**I**−**II**) or $Au_{10}S_4^-$ (**I**−**III**) can be clearly seen, allowing identification of isomer structures once experimental spectra are available.

Interestingly, some clusters on different routes (**1** and **6**) exhibit very similar shapes. For example, the $Au_7S_3^-$, $Au_9S_4^-$, $Au_{10}S_5^-$, and $Au_{11}S_5^-$ exhibit tetrahedron, pyramid, and triangular prism-like structures, which are similar to the structure of iso-atomic-number clusters $Au_6S_4^-$, $Au_8S_5^-$, $Au_9S_6^-$, and $Au_{10}S_6^-$, respectively, with one vertex S atom being replaced by an Au atom. The S−Au−S and Au−Au−S are two types of polyhedron edges. However, the Au−Au−S edge only appears in routes **6**, in which,the ratio of Au:S is greater than 3:2 and the cluster size is very small ($m + n < 15$). A reason for the appearance of the Au−Au−S edge is because each S atom tends to bond with three Au atoms. When the ratio of Au:S is greater than 3:2, all the S atoms are used up to form the S−Au−S edges and to maximize the number of S−Au−S edges. As a result, added Au atoms will form a small cluster to fit in existing framework built from the S−Au−S units, and eventually lead to the formation of Au−Au−S edges.

From the six evolution routes described above, three basic size-evolution rules can be summarized for the smaller $Au_mS_n^-$ clusters (*m* from 1 to 15), which are dependent on the Au/S ratio and cluster size:

(i) When cluster size is small ($m + n < 16$) and the Au:S ratio is less than or equal to 3:2, the structural evolution of cluster follows a simple edge-to-face growth mechanism, where the edge and face refer to the linear S−Au−S segment and triangular Au_3S_3 or square Au_4S_4 unit, respectively (Figure 1a). That is, *adding Au or S atom to the monoanionic $Au_mS_n^-$ cluster can lead to the formation of the S−Au−S edges and then to the stable triangular or square faces (Au_3S_3 or Au_4S_4)*. In general, the structural evolution of $Au_mS_n^-$ clusters from the linear AuS_2^- to hollow polyhedral structures (such as $Au_6S_4^-$, $Au_9S_6^-$, and $Au_{12}S_8^-$) is going through three basic steps: (1) the formation of a disulfide

bond with added S atom (for example, steps $Au_6S_4^- \rightarrow Au_6S_5^-$, $Au_8S_5^- \rightarrow Au_8S_6^- \rightarrow Au_8S_7^-$, and $Au_9S_6^- \rightarrow Au_9S_7^- \rightarrow Au_9S_8^-$, *etc.*), (2) insertion of an Au atom into the disulfide bond or two separated S atoms to form an S−Au−S edge (for example, steps $Au_5S_4^- \rightarrow Au_6S_4^-$, $Au_9S_8^- \rightarrow Au_{10}S_8^- \rightarrow Au_{11}S_8^- \rightarrow Au_{12}S_8^-$, *etc.*), and (3) repeating steps 1 and 2 to form either a triangular (Au_3S_3) or square (Au_4S_4) face.

(ii) If cluster size is small ($m + n < 16$) and the Au:S ratio is larger than 3:2, a modified edge-to-face mechanism is suggested. Here the edge is either Au−Au−S or S−Au−S and the Au_4S_2 and Au_5S_3 become basic triangular and square face. This modified edge-to-face evolution mechanism leads to formation of hollow polyhedron structures with mixed Au and S vertexes (such as $Au_7S_3^-$ and $Au_{10}S_5^-$ in route **6**).

(iii) Once the polyhedron structures are formed through the edge-to-face evolution steps, they can act as motifs for the formation of core-stacked and face-capped structures with a further increase of Au atoms (for example, the steps $Au_9S_6^- \rightarrow Au_{10}S_6^- \rightarrow Au_{11}S_6^-$, $Au_{10}S_5^- \rightarrow Au_{11}S_5^-$, and $Au_{12}S_8^- \rightarrow Au_{13}S_8^-$). Such tendency is consistent with the finding of the "core-in-cage" structure for $Au_{25}S_{12}^-$, $Au_{23}S_{11}^-$, and $Au_{27}S_{13}^-$.[46]

Also, a rule for the formation of hollow polyhedron structures is concluded for the Au_mS_n cluster at smaller sizes, for example, $m < 15$. Careful examination of the hollow polyhedral structures of $Au_6S_4^-$, $Au_9S_6^-$, and $Au_{12}S_8^-$ in Figure 1b indicates that these three clusters have common structural features such that the S atoms occupy all the vertex positions while all Au atoms are located in the middle of the edges. A criterion that the Au/S ratio should be 3:2 is postulated as the necessary condition for the formation of shared 3-coordinated S atom vertex, hollow polyhedral structures. According to this criterion, $Au_{15}S_{10}^-$ would be the next hollow polyhedral cluster with a shared 3-coordinated S atom vertex. To confirm this, we carry out a basin-hopping search on the $Au_{15}S_{10}^-$. This search and additional *ab initio* calculations at different levels indicate that the $Au_{15}S_{10}^-$ indeed exhibits a quasi-pentagonal prism structure with 10 vertex S atoms and 15 S−Au−S edges as shown in Figure 1c, which confirms the 3:2 ratio (Au/S) criterion. Other clusters such as $Au_7S_5^-$, $Au_{10}S_6^-$, $Au_{11}S_6^-$, and $Au_{12}S_7^-$ however do not show hollow and regular polyhedral structures as their Au/S ratio does not satisfy the 3:2 rule even though they also possess 3-coordinated S atoms as vertexes.

We conclude that the key stabilization mechanism for the hollow polyhedral structures in the $Au_mS_n^-$ clusters stems from the high stability of the S−Au−S and Au−Au−S building units. The formation energy (E_{form}) of $Au_mS_n^-$ at each evolution step is computed and listed in Figure 1b. From Figure 1b, the average E_{form} in one route is generally less than that between two different routes. For example, large E_{form} (>4.0 eV) is found between two different routes when the nearest-neighboring clusters have significant structural difference, for example, 4.28 eV between $Au_6S_3^-$ (route **6**) and $Au_6S_4^-$ (route **1**), and 4.04 eV between $Au_9S_5^-$ (route **3**) and $Au_9S_6^-$ (route **1**).

TABLE 1. Point Group (PG) Symmetry and HOMO−LUMO (H−L) Gap (in Unit of eV) of Selected Neutral and Monoanonic Au_mS_n Clusters[a]

	Au_6S_4	$Au_9S_5^-$	$Au_9S_6^-$	$Au_{12}S_8$	$Au_{15}S_{10}^-$
PG	S_4	C_{4v}	C_{2v}	D_{4h}	C_s
H−L gap	0.64	1.37	0.51	0.95	1.24

[a] Calculations are done at TPSS//cc-pVTZ (for S atom) and cc-pVTZ-PP (for Au atom) levels.

The tetrahedron, triangular prism, cuboctahedron, and pentagonal prism are a class of 3-connected polyhedral structures, which are consistent with the structural prediction of the 5*n* electron rule based on Wade and Mingos' skeleton electron pair approach.[4] In fact, the total number of valence electrons in neutral Au_6S_4, Au_9S_6, $Au_{12}S_8$, and $Au_{15}S_{10}$ are 30, 45, 60, and 75, respectively. We note that the neutral Au_6S_4, Au_9S_6, $Au_{12}S_8$, and $Au_{15}S_{10}$ clusters have the same polyhedron structure as their anionic counterparts. The gap between the highest occupied molecular orbital and the lowest unoccupied molecular orbital (HOMO−LUMO gap) of the neutral Au_6S_4, $Au_{12}S_8$, and monoanionic $Au_9S_6^-$ and $Au_{15}S_{10}^-$ are 0.64, 0.95, 0.51, and 1.24 eV, respectively (see Table 1). In the polyhedral clusters $Au_6S_4^-$, $Au_9S_6^-$, $Au_{12}S_8^-$, and $Au_{15}S_{10}^-$, some short Au−Au covalent bonds (less than 2.8 Å) are found in certain faces of polyhedral structures, which lead to lower symmetry (*cf.* Table 1), compared to the expected perfect polyhedral symmetry (T_d, D_{3h}, O_h, and D_{5h} for tetrahedron, triangular prism, cubahedron, and pentagonal prism, respectively). Here, the structure predicted for the $Au_{12}S_8^-$ anion is in agreement with previous experiments which showed a near-cubic geometry (O_h) polyanionic Au(I) thioaurate $[Au_{12}S_8]^{4-}$ in the solid crystal form.[64] However, the neighboring Au atoms are separated from each other with relatively large distances (>3.0 Å) in the $[Au_{12}S_8]^{4-}$, in contrast to the D_{4h} symmetry of the neutral $Au_{12}S_8$ and monoanionic $Au_{12}S_8^-$. The LUMOs of neutral $Au_{12}S_8$ are analyzed at TPSS//cc-pVTZ level as shown in Figure 2. One may find the two degenerated LUMOs in $Au_{12}S_8$ are contributed mainly from the antibonding Au−Au orbitals. The addition of extra four electrons to $Au_{12}S_8$ is expected to fill the antibonding Au−Au orbitals and therefore weaken the Au−Au covalent bond, which results in a near-cubic structure of $[Au_{12}S_8]^{4-}$.

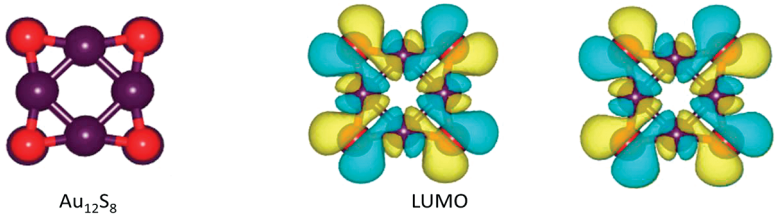

Figure 2. Degenerated LUMOs of neutral $Au_{12}S_8$ (computed at the TPSS//cc-pVTZ level).

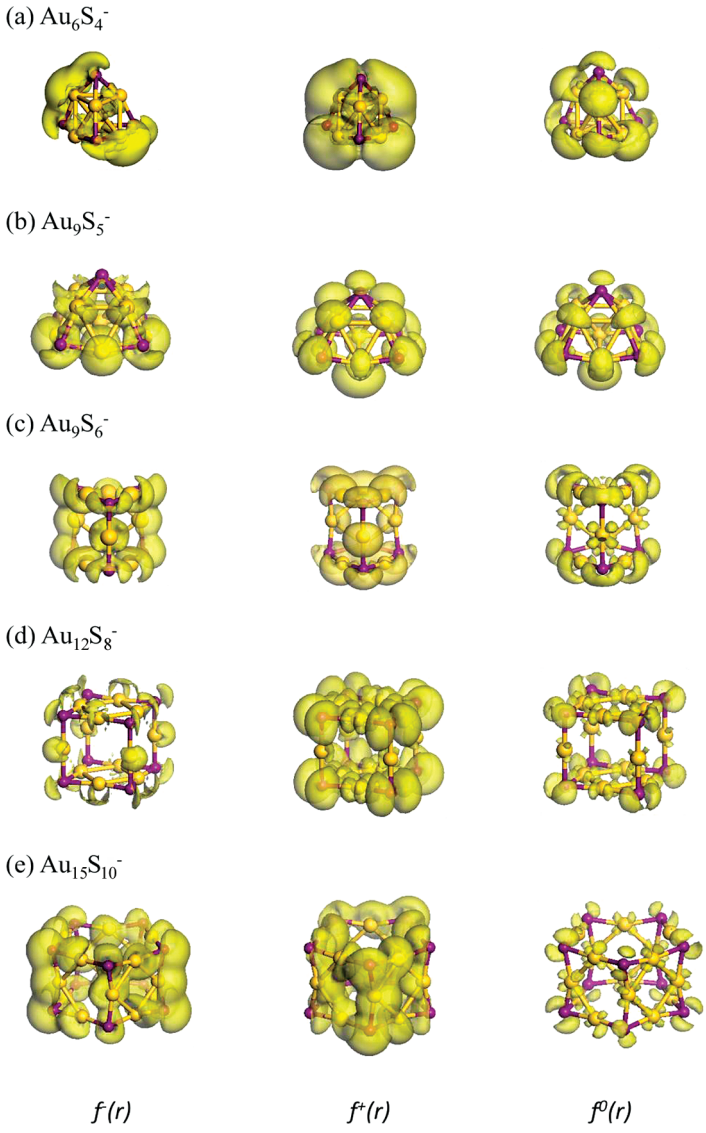

Figure 3. Iso-surface of Fukui functions $f^-(r)$, $f^+(r)$, and $f^0(r)$ calculated at the PBE/DND level. The iso-surface value is 0.006.

We also studied the chemical reactivity of these hollow polyhedron structures by computing the Fukui functions.[65] Specifically, the Fukui functions measure the sensitivity of the charge density $\rho(r)$ with respect to the loss or gain of electrons *via* the equations:

$$f^+(r) = (\rho N + \Delta N(r) - \rho_N(r))/\Delta N$$

$$f^-(r) = (\rho N(r) - \rho N - \Delta N(r))/\Delta N$$

$$f^0(r) = (f^+(r) + f^-(r))/2$$

where $f^+(r)$ measures changes in the electron density when the molecule (or cluster) gains electrons, thereby providing a description of reactivity with respect to nucleophilic attack. In contrast, $f^-(r)$ measures the reactivity with respect to the electrophilic attack (loss of electrons). The $f^0(r)$, which is the average of $f^+(r)$ and $f^-(r)$, describes the radical attack. In Figure 3, the iso-surface of $f^-(r)$, $f^+(r)$, *and* $f^0(r)$ of optimized $Au_6S_4^-$, $Au_9S_5^-$, $Au_9S_6^-$, $Au_{12}S_8^-$, and $Au_{15}S_{10}^-$ clusters are plotted, respectively, with an iso-surface value of 0.006.

Here, we use the PBE functional and DND basis set implemented in the DMol^3 program. The iso-surface can be interpreted as a reactive surface. As shown in Figure 3, all five cluster anions exhibit a fairly large contour of $f^+(r)$ iso-surface, indicating that these species all process relative high reactivity with respect to the nucleophilic attack. However, these hollow polyhedrons likely have different reactivity subjected to the electrophilic attack. The relatively low spatial distribution of $f^-(r)$ iso-surface on the $Au_{12}S_8^-$ suggests its relatively low reactivity regarding the electrophilic attack, compared to other polyhedron structures. Similarly, we can conclude that the $Au_{12}S_8^-$ and $Au_{15}S_{10}^-$ are relatively stable upon the radical attack due to their relatively low spatial distribution of $f^0(r)$ iso-surface. Our conclusion, to some extent, is consistent with a previous finding of highly stable near-cubic polyanionic Au(I) thioaurate $[Au_{12}S_8]^{4-}$.[64]

We now discuss our computational findings in the light of recent MS experiments. In their ion-mobility MS spectrum of $Au_{25}(SCH_2CH_2Ph)_{18}$, Dass *et al*. detected a series of fragment $Au_mS_n^-$ anions, in which $Au_{13}S_8^-$, $Au_{12}S_8^-$, $Au_{11}S_6^-$, $Au_{10}S_6^-$, $Au_9S_6^-$, and $Au_6S_4^-$ showed high abundance.[43] These magic-number clusters were also observed in high abundance in the MALDI/LDI MS of two different thiolated gold clusters made with dithiols.[42−45] From Figure 1b, these clusters are predicted to possess the polyhedron structures such as tetrahedron ($Au_6S_4^-$), triangular prism with or without encapsulated Au atom ($Au_{11}S_6^-$, $Au_{10}S_6^-$, or $Au_9S_6^-$), and cuboctahedron with or without encapsulated Au atom ($Au_{13}S_8^-$ or $Au_{12}S_8^-$). The relative high stabilities of hollow and encapsulated structures of these polyhedron clusters suggest they may be used to capsulate a heteroatom, replacing the inner Au atom, resulting in new properties or new superatoms. Such a study on the doping of heteroatom is underway.

In conclusion, we present an *ab initio* computational evidence of hollow or one-atom-centered polyhedral structures for many $Au_mS_n^-$ clusters observed in recent mass spectrometry experiments.[41−45] On the basis of the obtained low-lying structures with different Au/S ratios, an edge-to-face size-evolution rule is proposed to understand structural evolution of the clusters from simple S−Au−S edges to the quasi-polyhedron structures. The robustness of the polyhedral structures can be attributed to the high stability of S−Au−S and Au−Au−S structural unit and may be understood from Wades and Mingos' 5*n* electron rule. A 3:2 Au/S ratio is suggested for the formation of hollow polyhedron structures in the small-sized Au_mS_n clusters.

COMPUTATIONAL METHODS

Here, we employ the basin-hopping (BH) global-optimization method,[53] for which the potential energy and energy gradient are computed using the density-functional theory (DFT) methods[51,52] with a gradient-corrected functional (*i.e*., the Perdew−Burke−Ernzerhof (PBE) exchange-correlation functional,[54] implemented in the DMol^3 program[55]). All-electron *d*-polarization function included double-numerical (DND) basis set is selected. The BH−DFT approach (at the PBE/DND level) has proven to be efficient and yet cost-effective to attain reasonably accurate potential-energy surfaces (PES) for metal and semiconductor clusters. Previously, we have used this approach to explore structures of medium-sized anionic gold and neutral silicon clusters.[56,57] In practice, the BH algorithm comprises the Monte Carlo (MC) "random walks"[66] in conjunction with local optimization to locate local minima in the PES. Once a local minimum is located, the next MC step is to generate a new configuration on the PES. In the MC step, both Au and S atoms in a cluster can be considered as core atoms and moved randomly within a certain radius. The new configuration of the cluster is then fully optimized at the PBE/DND level of theory. Typically, for the clusters considered in this work, the BH-DFT search consistently yields a set of low-lying isomers within 200−500 MC steps.

Next, the set of low-lying isomer structures obtained from the BH−DFT/PBE search are reoptimized (with vibrational frequencies calculated) using the TPSS[58] exchange-correlation functional and a larger SDD basis set, implemented in the Gaussian 03 package.[59] The TPSS functional has been recently proven to be more accurate, compared to the PBE functional, in resolving relative stability of small-sized gold clusters.[60] For low-lying isomers, if the energy difference from the lowest-lying isomer is less than 0.2 eV (calculated at the TPSS//SDD level), their structures are further optimized (with frequencies calculated) at the TPSS//cc-pVTZ (for S atoms)//cc-pVTZ-PP(for Au atoms) level of theory. Note that both SDD and cc-pVTZ-PP basis sets for Au atoms are scalar relativistic effective-core potential basis. Lastly, single-point energy is evaluated using the Møller−Plesset second-order perturbation,[61,62] that is, MP2//cc-pVTZ (for S atom)//cc-pVTZ-PP (for Au atom) level of theory, based on the geometries from the TPSS//cc-pVTZ(for S)//cc-pVTZ-PP(for Au) optimization, for those isomers with energy being within 0.1 eV from the lowest-lying isomer. If both the TPSS/cc-pVTZ and MP2/cc-PVTZ//TPSS/cc-pVTZ calculations give rise to a consistent lowest-energy isomer, this isomer is most likely the global minimum. However, if the two levels of theory give rise to different lowest-energy isomers, then the lowest-energy isomer based on the MP2 calculation is tentatively assigned as the global minimum in this study (see Supporting Information). The true global minimum requires calculations at high-level coupled-cluster theory,[67] which is beyond the scope of this study.

Acknowledgment. Y.P. is partially supported by the Academic Leader Program in Xiangtan University. X.C.Z. is supported by grants from NSF (DMR-0820521, EPS-1010094), ARO (W911NF1020099), the Nebraska Research Initiative, and a seed grant from Nebraska Public Power District through the Nebraska Center for Energy Sciences Research, and by the University of Nebraska Holland's Computing Center. D.J. is supported by the Division of Chemical Sciences, Geosciences, and Biosciences, Office of Basic Energy Sciences, U.S. Department of Energy. Discussion with A. Dass, Z. F. Chen, and G. L. Wang was appreciated. This research also used resources of the National Energy Research Scientific Computing Center, which is supported by the Office of Science of the U.S. Department of Energy under Contract No. DE-AC02-05CH11231.

Supporting Information Available: Isomer structures and the relative electronic energies of $Au_mS_n^-$ isomers. Vertical detachment energy and computed photoelectron spectra of anionic

clusters and Cartesian coordinate of $Au_9S_5^-$, $Au_6S_4^-$, $Au_9S_6^-$, $Au_{12}S_8^-$, and $Au_{15}S_{10}^-$. This material is available free of charge *via* the Internet at http://pubs.acs.org.

REFERENCES AND NOTES

1. Alvarez, S. Polyhedra in (Inorganic) Chemistry. *Dalton Trans.* **2005,** 2209–2233.
2. Jena, P.; Castleman, A. W., Jr. Clusters: A bridge across the Disciplines of Physics and Chemistry. *Proc. Natl. Acad. Sci. U.S.A.* **2006,** *103*, 10560–10569.
3. Wade, K. Structural and Bonding Pattern in Cluster Chemistry. *Adv. Inorg. Chem. Radio Chem.* **1976,** *18*, 1–66.
4. Mingos, D. M. Polyhedral Skeletal Electron Pair Approach. *Acc. Chem. Res.* **1984,** *17*, 311–319.
5. Corbett, J. D. Polyanionic Clusters and Networks of the Early p-Element Metals in the Solid State: Beyond the Zintl Boundary. *Angew. Chem., Int. Ed.* **2000,** *39*, 670–690.
6. Fässler, T. F.; Hoffmann, S. D. Endohedral Zintl Ions: Intermetalloid Clusters. *Angew. Chem., Int. Ed.* **2004,** *43*, 6242–6247.
7. Schnepf, A. Novel Compounds of Elements of Group 14: Ligand-Stabilized Clusters with "Naked" Atoms. *Angew. Chem. Int. Ed.* **2004,** *43*, 664–666.
8. Spiekermann, A.; Hoffmann, S. D.; Fässler, T. F. The Zintl Ion $[Pb_{10}]^{2-}$: A Rare Example of a Homoatomic *closo* Cluster. *Angew. Chem., Int. Ed.* **2006,** *45*, 3459–3462.
9. Cui, L.-F.; Huang, X.; Wang, L.-M; Zubarev, D. Y.; Boldyrev, A. I.; Li, J.; Wang, L. S. Sn_{12}^{2-}: Stannaspherene. *J. Am. Chem. Soc.* **2006,** *128*, 8390–8391.
10. Cui, L.-F.; Huang, X.; Wang, L.-M; Zubarev, D. Y.; Li, J.; Wang, L. S. Pb_{12}^{2-}: Plumbaspherene. *J. Phys. Chem.* **2006,** *110*, 10169–10172.
11. Esenturk, E. N.; Fettinger, J.; Eichhorn, B. The Pb_{12}^{2-} and Pb_{10}^{2-} Zintl Ions and the $M@Pb_{12}^{2-}$ and $M@Pb_{10}^{2-}$ Cluster Series Where M = Ni, Pd, Pt. *J. Am. Chem. Soc.* **2006,** *128*, 9178–9186.
12. Bulusu, S.; Li, X.; Wang, L. S.; Zeng, X. C. Evidence of Hollow Gold Cages. *Proc. Natl. Acad. Sci. U.S.A.* **2006,** *103*, 8326–8330.
13. Pyykkö, P. Relativistic Effects in Structural Chemistry. *Chem. Rev.* **1988,** *88*, 563–594.
14. Pyykkö, P. Theoretical Chemistry of Gold. *Angew. Chem., Int. Ed.* **2004,** *43*, 4412–4456.
15. Pyykkö, P. Theoretical Chemistry of Gold II. *Inorg. Chim. Acta* **2005,** *358*, 4113–4130.
16. Johansson, M. P.; Sundholm, D.; Vaara, J. Au_{32}: A 24-Carat Golden Fullerene. *Angew. Chem., Int. Ed.* **2004,** *43*, 2678–2681.
17. Gu, X.; Ji, M.; Wei, S. H.; Gong, X .G. Au_N clusters (N = 32, 33, 34, 35): Cage-like Structures of Pure Metal Atoms. *Phys. Rev. B* **2004,** *70*, 205401-1–205401-5.
18. Gao, Y.; Zeng, X. C. Au_{42}: An Alternative Icosahedral Golden Fullerene Cage. *J. Am. Chem. Soc.* **2005,** *127*, 3698–3699.
19. Wang, J.; Jellinek, J.; Zhao, J.; Chen, Z.; King, R. B.; Schleyer, P. v. R. Hollow Cages *versus* Space-Filled Structures for Medium-Sized Gold Clusters: The Spherical Aromaticity of the Au_{50} Cage. *J. Phys. Chem. A* **2005,** *109*, 9265–9269.
20. Johannsson, M. P.; Vaara, J.; Sundholm, D. Exploring the Stability of Golden Fullerenes. *J. Phys. Chem. C* **2008,** *112*, 19311–19315.
21. Ferrando, R.; Barcaro, G.; Fortunelli, A. Surface-Supported Gold Cages. *Phys. Rev. Lett.* **2009,** *102*, 216102–1−4.
22. Kruger, S.; Stener, M.; Mayer, M.; Nortemann, F.; Rosch, N. Gold−Thiolate Complexes: A Density Functional Study of Geometry and Electronic Structure. *J. Mol. Struct. (Theochem)* **2000,** *527*, 63–74.
23. Brust, M.; Walker, M.; Bethell, D.; Schiffrin, D. J.; Whyman, R. Synthesis of Thiol-Derivatised Gold Nanoparticles in a Two-Phase Liquid−Liquid System. *J. Chem. Soc., Chem. Commum.* **1994,** 801–802.
24. Jadzinsky, P. D.; Calero, G.; Ackerson, C. J.; Bushnell, D. A.; Kornberg, R. D. Structure of a Thiol Monolayer−Protected Gold Nanoparticle at 1.1 Å Resolution. *Science* **2007,** *318*, 430–433.
25. Heaven, M. W.; Dass, A.; White, P. S.; Holt, K. M.; Murray, R. W. Crystal Structure of the Gold Nanoparticle $[N(C_8H_{17})_4][Au_{25}(SCH_2CH_2Ph)_{18}]$. *J. Am. Chem. Soc.* **2008,** *130*, 3754–3755.
26. Akola, J.; Walter, M.; Whetten, R. L.; Häkkinen, H.; Grönbeck, H. On the Structure of Thiolate-Protected Au_{25}. *J. Am. Chem. Soc.* **2008,** *130*, 3756–3757.
27. Zhu, M.; Aikens, C. M.; Hollander, F. J.; Schatz, G. C.; Jin, R. Correlating the Crystal Structure of A Thiol-Protected Au_{25} Cluster and Optical Properties. *J. Am. Chem. Soc.* **2008,** *130*, 5883–5885.
28. Dass, A. Mass Spectrometric Identification of $Au_{68}(SR)_{34}$ Molecular Gold Nanoclusters with 34-Electron Shell Closing. *J. Am. Chem. Soc.* **2009,** *131*, 11666–11667.
29. Lopez-Acevedo, O.; Akola, J.; Whetten, R. L.; Grönbeck, H.; Häkkinen, H. Structure and Bonding in the Ubiquitous Icosahedral Metallic Gold Cluster $Au_{144}(SR)_{60}$. *J. Phys. Chem. C* **2009,** *113*, 5035–5038.
30. Pei, Y.; Gao, Y.; Zeng, X. C. Structural Prediction of Thiolate-Protected Au_{38}: A Face-Fused Bi-icosahedral Au Core. *J. Am. Chem. Soc.* **2008,** *130*, 7830–7832.
31. Tsunoyama, H.; Nickut, P.; Negishi, Y.; Al-Shamery, K.; Matsumoto, Y.; Tsukuda, T. Formation of Alkanethiolate-Protected Gold Clusters with Unprecedented Core Sizes in the Thiolation of Polymer-Stabilized Gold Clusters. *J. Phys. Chem. C* **2007,** *111*, 4153–4158.
32. Jiang, D. E.; Walter, M.; Akola, J. On the Structure of a Thiolated Gold Cluster: $Au_{44}(SR)_{28}^{2-}$. *J. Phys. Chem. C* **2010,** *114*, 15883–15889.
33. Jiang, D. E.; Whetten, R. L.; Luo, W. D.; Dai, S. The Smallest Thiolated Gold Superatom Complexes. *J. Phys. Chem. C* **2009,** *113*, 17291–17295.
34. Gao, Y.; Shao, N.; Zeng, X. C. *Ab Initio* Study of Thiolate-Protected Au_{102} Nanocluster. *ACS Nano* **2008,** *2*, 1497–1503.
35. Pei, Y.; Gao, Y.; Shao, N.; Zeng, X. C. Thiolate-Protected $Au_{20}(SR)_{16}$ Cluster: Prolate Au_8 Core with New $[Au_3(SR)_4]$ Staple Motif. *J. Am. Chem. Soc.* **2009,** *131*, 13619–13621.
36. Qian, H.; Eckenhoff, W. T.; Zhu, Y.; Pintauer, T.; Jin, R. Total Structure Determination of Thiolate-Protected Au_{38} Nanoparticles. *J. Am. Chem. Soc.* **2010,** *132*, 8280–8282.
37. Wiseman, M. R.; Marsh, P. A.; Bishop, P. T.; Bridsdon, B. J.; Mahon, M. F. Homoleptic Gold Thiolate Catenanes. *J. Am. Chem. Soc.* **2000,** *122*, 12598–12599.
38. Negishi, Y.; Nobusada, K.; Tsukuda, T. Glutathione-Protected Gold Clusters Revisited: Bridging the Gap between Gold(I)−Thiolate Complexes and Thiolate-Protected Gold Nanocrystals. *J. Am. Chem. Soc.* **2005,** *127*, 5261–5270.
39. Shao, N.; Pei, Y.; Gao, Y.; Zeng, X. C. Onset of Double Helical Structure in Small-Sized Homoleptic Gold Thiolate Clusters. *J. Phys. Chem. A* **2009,** *113*, 629–632.
40. Grönbeck, H.; Whetten, R. L.; Häkkinen, H. Theoretical Characterization of Cyclic Thiolated Gold Clusters. *J. Am. Chem. Soc.* **2006,** *128*, 10268–10275.
41. Wu, Z.; Jin, R. C. Stability of the Two Au−S Binding Modes in $Au_{25}(SG)_{18}$ Nanoclusters Probed by NMR and Optical Spectroscopy. *ACS Nano* **2009,** *3*, 2036–2042.
42. Dass, A.; Dubay, G. B.; Fields-Zinna, C. A.; Murray, R. W. FAB Mass Spectrometry of $Au_{25}(SR)_{18}$ Nanoparticles. *Anal. Chem.* **2008,** *80*, 6845–6849.
43. Angel, L. A.; Majors, L. T.; Dharmaratne, A. C.; Dass, A. Ion Mobility Mass Spectrometry of $Au_{25}(SCH_2CH_2Ph)_{18}$ Nanoclusters. *ACS Nano* **2010,** *4*, 4691–4700.
44. Negishi, Y.; Tsukuda, T. One-Pot Preparation of Subnanometer-Sized Gold Clusters *via* Reduction and Stabilization by meso-2,3-Dimercaptosuccinic Acid. *J. Am. Chem. Soc.* **2003,** *125*, 4046–4047.
45. Tang, Z. H.; Xu, B.; Wu, B. H.; Robinson, D.; Bokossa, N.; Wang, G. L. Monolayer Reactions of Protected Au Nanoclusters with Monothiol Tiopronin and 2,3-Dithiol Dimercaptoproponic Sulfonate. Unpublished work.
46. Jiang, D. E.; Walter, S.; Dai, S. Gold Sulfide Nanoclusters: A Unique Core-in-Cage Structure. *Chem.—Eur. J.* **2010,** *16*, 4999–5003.

47. Zhai, H.-J.; Burgel, C.; Bonacic-Koutecky, V.; Wang, L. S. Probing the Electronic Structure and Chemical Bonding of Gold Oxides and Sulfides in AuO_n^- and AuS_n^- (n = 1, 2). *J. Am. Chem. Soc.* **2008,** *130*, 9156–9167.
48. Wang, X.; Liang, B.; Andrews, L. Infrared Spectra and Density Functional Theory Calculations of Coinage Metal Disulfide Molecules and Complexes. *Dalton Trans.* **2009,** 4190–4198.
49. Woldeghebriel, H.; Kshisagar, A. How Cationic Gold Clusters Respond to a Single Sulfur Atom. *J. Chem. Phys.* **2007,** *127*, 224708-1–224708-9.
50. Bravo-Perez, G.; Garzón, I. L. *Ab Initio* Study of Small Au_nS, (n = 1−5) and Au_nS_2, (n = 1−4) Clusters. *J. Mol. Struc. (THEOCHEM)* **2002,** *619*, 79–89.
51. Hohenberg, P. Inhomogeneous Electron Gas. *Phys. Rev. B* **1964,** *136*, 864–871.
52. Kohn, W.; Sham, L. J. Self-Consistent Equations Including Exchange and Correlation Effects. *Phys. Rev. A* **1965,** *140*, 1133–1138.
53. Wales, D. J.; Scheraga, H. A. Global Optimization of Clusters, Crystals, and Biomolecules. *Science* **1999,** *285*, 1368–1372.
54. Perdew, J. P.; Burke, K.; Ernzerhof, M. Generalized Gradient Approximation Made Simple. *Phys. Rev. Lett.* **1996,** *77*, 3865–3868.
55. Delley, B. An All-Electron Numerical Method for Solving the Local Density Functional for Polyatomic Molecules. *J. Chem. Phys.* **1990,** *92*, 508–517 (DMOl3 is available from Accelrys, San Diego).
56. Shao, N.; Huang, W.; Gao, Y.; Wang, L.-M.; Li, X.; Wang, L.-S.; Zeng, X. C. Probing the Structural Evolution of Medium-Sized Gold Clusters: Au_n^- (n = 27−35). *J. Am. Chem. Soc.* **2010,** *132*, 6596–6605.
57. Bai, J.; Cui, L.-F.; Wang, J. L.; Yoo, S.; Li, X.; Jellinek, J.; Koehler, C.; Frauenheim, Th.; Wang, L.S.; Zeng, X.C. Structural Evolution of Anionic Silicon Clusters Si_N ($20 < N < 45$). *J. Phys. Chem. A* **2006,** *110*, 908–912.
58. Tao, J.; Perdew, J. P.; Staroverov, V. N.; Scuseria, G. E. Climbing the Density Functional Ladder: Nonempirical Meta−Generalized Gradient Approximation Designed for Molecules and Solids. *Phys. Rev. Lett.* **2003,** *91*, 146401-1–146401-4.
59. Frisch, M. M. J.; Trucks, G. W.; Schlegel, H. B.; Scuseria, G. E.; Robb, M. A.; Cheeseman, J. R.; Montgomery, J. A., Jr.; Vreven, T.; Kudin, K. N.; Burant, J. C.; *et al. Gaussian 03*, revision C.02; Gaussian, Inc.: Wallingford, CT, 2004.
60. Johansson, M. P.; Lechtken, A.; Schooss, D.; Kappes, M. M.; Furche, F. 2D−3D Transition of Gold Cluster Anions Resolved. *Phys. Rev. A* **2008,** *77*, 053202-1–053202-7.
61. Head-Gordon, M.; Pople, J. A.; Frisch, M. J. MP2 Energy Evaluation by Direct Methods. *Chem. Phys. Lett.* **1988,** *153*, 503–506.
62. Frisch, M. J.; Head-Gordon, M.; Pople, J. A. A Direct MP2 Gradient Method. *Chem. Phys. Lett.* **1990,** *166*, 275–280.
63. Wu, Z. K; Jiang, D. E.; Lanni, E; Bier, M. E.; Jin, R. C. Sequential Observation of $Ag_nS_4^-$ ($1 \leq n \leq 7$) Gas Phase Clusters in MS/MS and Prediction of Their Structures. *J. Phys. Chem. Lett.* **2010,** *1*, 1423–1427.
64. Marbach, G.; Strähle, J. Synthesis and Crystal Structure of $[Ph_4As]_4[Au_{12}S_8]$, a Distorted Cubane-like Thioaurate(I). *Angew. Chem., Int. Ed.* **1984,** *23*, 715–716.
65. Parr, R. G.; Yang, W. *Density-Functional Theory of Atoms and Molecules*; Oxford University Press: New York, 1989.
66. Ferrando, R.; Fortunelli, A.; Jonhston, R. L. Search for the Optimum Structures of Alloy Nanoclusters. *Phys. Chem. Chem. Phys.* **2008,** *10*, 640–649.
67. Choi, Y. C.; Kim, W. Y.; Lee, H. M.; Kim, K. S. Neutral and Anionic Gold Decamers: Planar Structure with Unusual Spatial Charge−Spin Separation. *J. Chem. Theory Comput.* **2009,** *5*, 1216–1223.